International Journal of Applied Engineering Research ISSN 0973-4562 Volume 12, Number 23 (2017) pp. 13127-13136

Physical and Technical Restrictions of Materials Recognition by the Dual High Energy X-ray Imaging

Sergei P. Osipov[1]*, Sergei V. Chakhlov[1], Oleg S. Osipov[2], Suqi Li[3], Xiaoming Sun[3], Jianbin Zheng[3], Xiaowei Hu[3], Gaolong Zhang[3]

[1]National Research Tomsk Polytechnic University, 30, Lenin Avenue, Tomsk, 634050, Russian Federation.
[2]Solveig Multimedia, 3, Razvitiya avenue, Tomsk, 634021, Russian Federation.
[3]PowerScan LTD, Hanhua Office, #23, 1/F, West Xueqing Road, Haidian District Beijing, 100029, P.R. China.

Abstract

The paper presents physical and technical restrictions of the materials recognition of objects and their fragments using the dual energy method. It is shown that the recognition parameters for materials having different effective atomic numbers are similar within the detected thickness range of target objects. The correlation is shown between the bit capacity of the analog-to-digital converter and the thickness range of objects the materials of which are recognized correctly. The recommendations are given for the expanding the application area of the dual-energy method for the materials recognition.

Keywords: X-ray radiation, customs inspection, dual energy method, material recognition, analog-to-digital converter.

INTRODUCTION

The cargo inspection systems with the function of the materials recognition of objects and their fragments using the dual high energy method is one the most promising technologies of customs control [1-3]. Linear accelerators and betatrons are used in these inspection systems as the X-ray sources [4-6]. The distinctions of the dual high energy X-ray radiation, its interaction with the object materials and radiometric detector recordings generate a number of factors of physical and technical origins. These factors significantly affect the quality of recognition of large-size cargoes and their fragments provided by the dual-energy method [7]. A random nature of the high energy X-ray emission, interaction, and recording in combination with strict consumers' requirements for the efficiency or radiant power of customs inspection systems reduce the quality of the materials recognition of objects and their fragments [8, 9]. The simplest implementation technique of the materials recognition is the level line method [1, 7, 10, 11]. There is little information offered in the literature concerning physical and technical restrictions of the materials recognition of objects using this method.

The short description of the level line method for better understanding of the restriction origins and the ways of their elimination is presented below.

MATERIAL RECOGNITION OF OBJECTS AND THEIR FRAGMENTS USING THE HIGH ENERGY METHOD OF LEVEL LINES

First, the theoretical basics of the level line method will be described [8, 11-13]. The material recognition algorithm using the method of level lines includes several stages.

Digital radiographic imaging

At the first stage, two digital shadow radiographs are generated for two distinct energies E_L and E_H helping to determine the materials of L and H objects, where $E_L < E_H$. Hereinafter, L and H indices define the lower and the higher maximum X-ray energies, respectively. Images of L and H objects are integer matrices with $M \times N$ dimension.

$$\mathbf{L} = \{L_{mn} : m = 1...M;\ n = 1...N\},\ \mathbf{H} = \{H_{mn} : m = 1...M;\ n = 1...N\} \quad (1)$$

The values of L_{mn} and H_{mn} are taken from K range from 0 to 2^k-1, where k is the bit capacity of the analog-to-digital converter (ADC).

The digital radiographs of L and H objects are formed by a set of radiometric signals Y_L and Y_H. Let us introduce the following notation: a and b are the amplification factor and the level of self-noise of radiometric detector, respectively; P_L, P_H are radiant powers on the frontal area of detector; c_L, c_H are power-to-flux conversion factors; t_L, t_H are measurement times. Note, that for X-ray pulse sources, the measurement time depends on the number of pulses. Radiometric signals behind the target object with ρh mass thickness, the material of which has Z effective atomic number, are obtained as follows:

$$\begin{aligned} Y_L(\rho h, Z) &= ac_L P_L t_L \int_0^{E_L} \overline{E_{\text{ab}}(E)}\, f(E, E_L) \mathrm{e}^{-m(E,Z)\rho H} \varepsilon(E) dE + bt_L \\ Y_H(\rho h, Z) &= ac_H P_H t_H \int_0^{E_H} \overline{E_{\text{ab}}(E)}\, f(E, E_H) \mathrm{e}^{-m(E,Z)\rho H} \varepsilon(E) dE + bt_H \end{aligned} \quad (2)$$

where $\overline{E_{\text{ab}}(E)}$ is the average energy in the detector retained by the recorded photon with E energy; $f(E,E_L)$, $f(E,E_H)$ are X-ray energy spectrums; $m(E, Z)$ is the mass attenuation

coefficient; ε (*E*) is the detection efficiency for radiation energy *E*.

The correlation between the analog and digital signals can be written as

$$L(\rho h, Z) = \text{int}\left(\frac{Y_L(\rho h, Z)}{\Delta}\right)$$
$$H(\rho h, Z) = \text{int}\left(\frac{Y_H(\rho h, Z)}{\Delta}\right) \quad (3)$$

where *int* is the integral part of a number; Δ is the analog signal corresponding to the ADC unit. Δ value depends on ADC bit capacity and the measuring range of the analog signal with reference to the coefficient C_Δ<1 which considers the possible fluctuations and inhomogeneity of the amplification factor in radiometric detectors. Thus, the analog signal can be obtained from

$$\Delta = \frac{Y(0, Z)}{C_\Delta(2^k - 1)} \quad (4)$$

Calibration and linearization

The input of the calibration and linearization element receives four groups of signals. The first-group signals denoted as $L(\infty, Z)$ and $H(\infty, Z)$, are generated when the X-ray source is turned off. The second-group signals denoted as $L(0,Z)$ and $H(0,Z)$ are measured without the target object, *i.e.* signals travel through the air. The third-group includes $L(\rho h,Z)$ and $H(\rho h,Z)$ signals for measuring the object proper. Signals $L_R(\rho h,Z)$ and $H_R(\rho h,Z)$ of the fourth group do not depend on presence or absence of the target object. The notation $L_R(\rho h,Z)$ and $H_R(\rho h,Z)$ emphasizes their concurrent formation with either measuring signals or those travelling through the air and indicates that they are reference signals. The condition for reference signals to be positioned beyond the object shadow should be observed. The signals of the fourth group are required to reduce from-pulse-to-pulse fluctuations of X-ray radiation parameters.

A combination of calibration and linearization reduces to the sequence of computations described by

$$R_L(\rho h, Z) = \ln\frac{L(0,Z) - L(\infty,Z)}{L_R(0,Z) - L(\infty,Z)} - \ln\frac{L(\rho h,Z) - L(\infty,Z)}{L_R(\rho h,Z) - L(\infty,Z)}$$
$$R_H(\rho h, Z) = \ln\frac{H(0,Z) - H(\infty,Z)}{H_R(0,Z) - H(\infty,Z)} - \ln\frac{H(\rho h,Z) - H(\infty,Z)}{H_R(\rho h,Z) - H(\infty,Z)} \quad (5)$$

The values of $R_L(\rho h,Z)$ and $R_H(\rho h,Z)$ characterize the radiation length of the target object with ρh and Z parameters for maximum E_L and E_H radiation energies.

After calibration and linearization, integer matrices of L and H transform to R_L and R_H matrices.

Material recognition

In terms of the level line method, the materials recognition parameter Q is introduced in the following way:

$$Q\left(R_L(\rho H, Z)\right) = \frac{R_H(\rho H, Z)}{R_L(\rho H, Z)} \quad (6)$$

This equation considers Q parameter as a function of the radiation length of the target object for the lower maximum energy. This fact is important as it allows comparing the experimental and calibration values of the recognition parameter with regard for R_L value.

For the materials recognition based on the level line method, R_L and R_H images are used to generate the final X-ray image:

$$\mathbf{Q} = \left\{ Q_{mn} = \frac{R_{H\,mn}}{R_{L\,mn}} : m = 1...M;\ n = 1...N \right\} \quad (7)$$

The target object material in the point with coordinates (m, n) is relevant to a certain material if only the following condition is satisfied:

$$U_-(R_{L\,mn}) < Q_{mn} \le U_+(R_{L\,mn}) \quad (8)$$

where $U_-(R_{L\,mn})$, $U_+(R_{L\,mn})$ are the level lines for the relevant material.

The level lines are detected experimentally by the target object with regard for $Q(R_L(\rho h, Z)) = R_H(\rho h, Z)/R_L(\rho h, Z)$ dependence. The variation range for mass thickness and effective atomic numbers of the target object material and its fragments should correspond to the region of interest.

PHYSICAL AND TECHNICAL RESTRICTIONS OF MATERIALS RECOGNITION

In customs inspection, all materials of target objects are conventionally divided into four classes. Each class is represented by the certain type of materials. Thus, organic materials are represented by carbon, and materials of a low, medium and high effective atomic number – by aluminum, steel, and lead, respectively.

As an example, the target object fragments have Z_1 and Z_2 effective atomic numbers, where $Z_2 > Z_1$. Let us consider the whole theoretic variation range of their mass thicknesses, namely $0 \le \rho h < \infty$. In the analysis of $Q(R_L(\rho h, Z_1))$ and $Q(R_L(\rho h, Z_2))$ dependences, it is interesting to discriminate the materials fragments of low thickness and large-size cargos. It is obvious, that the equality of these dependences in some ρh_0 point excludes the possibility of correct recognition of materials having thickness close to ρh_0. Hence, a number of problems should be solved that can be formalized as

$$\begin{aligned}&1.\ \lim_{\rho h\to 0} Q(R_L(\rho h,Z))=?\\&2.\ \lim_{\rho h\to\infty} Q(R_L(\rho h,Z))=?\\&3.\ Q(R_L(\rho h_0,Z_1))=Q(R_L(\rho h_0,Z_2)),Z_1\neq Z_2,0\le\rho h_0<\infty,\ \ \rho h_0=?\end{aligned}\qquad(9)$$

The solution of the first two problems allows considering a physical capability of the materials recognition of small- and large-size cargos using the method of level lines. The solution of the third problem reveals the existence of thickness intervals of the target object for which the materials recognition is not physically realizable. For convenience, let us call these intervals and relevant points the intervals/points of uncertainty in materials recognition.

Ultimate values of recognition parameter for small-size objects

Using (2)-(6), we get the recognition parameter Q:

$$Q(R_L(\rho h,Z))=\begin{cases}\dfrac{m_{int}(E_H,\rho h,Z)}{m_{int}(E_L,\rho h,Z)},\ \rho h>0\\ \lim\limits_{\rho h\to 0}\dfrac{m_{int}(E_H,\rho h,Z)\rho h}{m_{int}(E_L,\rho h,Z)\rho h},\ \rho h\approx 0\end{cases}\qquad(10)$$

where $m_{int}(E_L, \rho h, Z)$, $m_{int}(E_H, \rho h, Z)$ are the integral mass attenuation coefficients of the material passed through the X-ray beam with an atomic number Z at maximum E_L and E_H energies.

Using (10), obtain

$$Q_0(E_L)=\lim_{\rho h\to 0} Q(R_L(\rho h,Z))=\frac{m_{diff}(E_H,0,Z)}{m_{diff}(E_L,0,Z)}\qquad(11)$$

where $m_{diff}(E_L, \rho h, Z)$, $m_{diff}(E_H, \rho h, Z)$ are the differential mass attenuation coefficients of X-ray radiation. The value of $m_{diff}(E_{max}, \rho h, Z)$ is defined as

$$m_{diff}(E_{max},\rho h,Z))=\frac{\int_0^{E_{max}}\overline{E_{ab}(E)}f(E,E_{max})m(E,Z)e^{-m(E,Z)\rho H}\varepsilon(E)dE}{\int_0^{E_{max}}\overline{E_{ab}(E)}f(E,E_{max})e^{-m(E,Z)\rho H}\varepsilon(E)dE}\qquad(12)$$

In (11) and (12) Schiff equation is used to describe the energy spectrum of X-ray radiation with allowance for the thickness of the attenuating filter [14, 15], while $m(E, Z)$ dependence is calculated in accordance with the database on the interaction between γ-radiation and substance [16, 17]. As for $\overline{E_{ab}(E)}$ dependence for scintillation detectors of different size, approximations [18] and data from the Laboratory of Analysis of Integral Experiments and Improvement of Nuclear Group Data [16] can be used.

According to (11), the analyzed ultimate values depend on such three parameters as E_L and E_H energies and Z effective atomic number. In Fig. 1, $Q_0(E_L)$ dependences are presented, the effective atomic number Z possesses values from {6; 13; 26; 82} range.

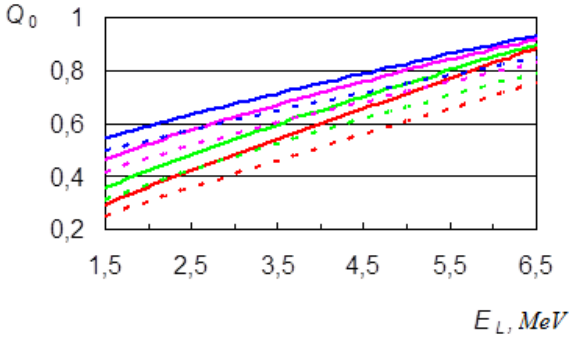

Figure 1: $Q_0(E_L)$ dependences: ——, - - - E_H=7.5 MeV, E_H=9 MeV, Z=6; ——, - - - E_H=7.5 MeV, E_H=9 MeV, Z=13; ——, - - - E_H=7.5 MeV, E_H=9 MeV, Z=26; ——, - - - E_H=7.5 MeV, E_H=9 MeV, Z=82.

According to Fig. 1, the express-evaluation can be carried out for the different recognition parameters of low-thickness objects made of carbon, aluminum, iron, and lead at specified values of E_L and E_H.

Ultimate values of recognition parameter for large-size objects

In solving the second problem from (9), there is no need to calculate the ultimate values at $\rho h\to\infty$. It is enough to limit to rather a large value, *e.g.* ρh=170 g/cm^2.

The integral mass attenuation coefficient of the material passed through the X-ray beam with an atomic number Z and mass thickness ρh at a maximum E_{max} energy is defined as

$$m_{int}(E_{max},\rho h,Z)=-\frac{1}{\rho h}\ln\frac{\int_0^{E_{max}}\overline{E_{ab}(E)}f(E,E_{max})e^{-m(E,Z)\rho H}\varepsilon(E)dE}{\int_0^{E_{max}}\overline{E_{ab}(E)}f(E,E_{max})\varepsilon(E)dE}\qquad(13)$$

Figure 2 shows the $Q_\infty(E_L)$ dependences for carbon, aluminum, steel and lead.

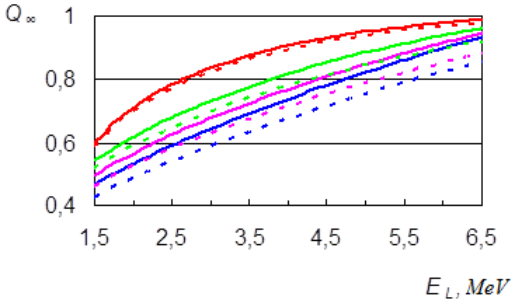

Figure 2: $Q_\infty(E_L)$ dependences: ——, - - - E_H=7.5 MeV, E_H=9 MeV, Z=6; ——, - - - E_H=7.5 MeV, E_H=9 MeV, Z=13; ——, - - - E_H=7.5 MeV, E_H=9 MeV, Z=26; ——, - - - E_H=7.5 MeV, E_H=9 MeV, Z=82.

Figure 2 proves the principal physical capability of correct materials recognition of large-size target objects using the level line method. It should be noted that the order of lines by the effective atomic number is opposite to that shown in Fig. 1. This allows us to suppose that there exists the mass thickness value of $\rho h = \rho h_0$ which is the solution of the third problem in (9).

Intervals of uncertainty in materials recognition

In order to get points and intervals of uncertainty in materials recognition, $Q(\rho h)$ dependencies were constructed for $Z \in \{6,13,26,82\}$. Figure 3 illustrates $Q(\rho h)$ dependencies for two pairs of E_L and E_H energies at 4-7.5 and 4.5-9 MeV. The mass thickness ρh ranges from 0 to 40 g/cm^2.

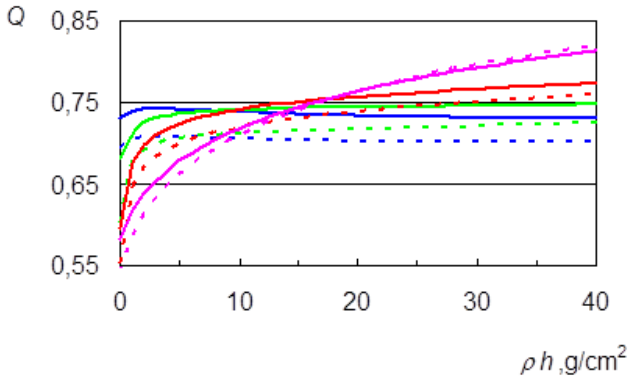

Figure 3: $Q(\rho h)$ dependences for E_L–E_H energy pairs: ——, - - - 4–7.5 and 4.5–9 MeVs, Z=6; ——, - - - 4–7.5 and 4.5–9 MeVs, Z=13; ——, - - - 4–7.5 and 4.5–9 MeVs, Z=26; ——, - - - 4–7.5 and 4.5–9 MeVs, Z=82.

According to Fig. 3, the correct recognition of materials with the atomic number not over 26 units and 5-15 g/cm^2 mass thickness range is rather uncertain. For the materials with a large atomic number the interval of uncertainty shifts to the region of large ρh values and reaches 20 g/cm^3. Notable, that the intervals of uncertainty considerably depend on the pair of maximum energies. Thus, for E_L-E_H energies of 4-7.5 MeV, the interval of uncertainty is much larger than that of E_L-E_H energies of 4.5-9 MeV.

On the strength of the specific importance of the abovementioned physical restriction of the recognition quality, a series of additional calculations was carried out to determine the intervals of uncertainty. Thus, their quantitative determination can be written as

$$\left|Q\left(R_L(\rho h, Z_1)\right) - Q\left(R_L(\rho h, Z_2)\right)\right| \le \delta \qquad (14)$$

where δ is the uncertainty level.

The calculation results for the intervals of uncertainly are given in Table 1 for δ=0.005.

Table 1: Intervals of uncertainly (ρh_-, ρh_+), g/cm^2, δ=0,005.

E_L, MeV	E_H, MeV	Z_2	Z_1		
			6	13	26
4	7.5	13	(5.2,12.5)		
		26	(7.8,10.9)	(7.6,13.1)	
		82	(12.5,14.4)	(13.6,15.9)	(15.6,19.2)
4.5	9	13	(3.9,8.5)		
		26	(5.6,7.6)	(5.5,9.1)	
		82	(8.9,10.1)	(9.7,11.2)	(11.1,13.6)

The intervals of uncertainly for 4-7.5 MeV E_L-E_H energies shift to the ρh increase as compared to that of 4.5-9 MeV E_L-E_H energies. The latter have considerably narrower intervals of uncertainly.

The theoretical rationale for the existence of points and intervals of uncertainty is proved by the experimental results described in works [19, 20].

Note. The presence of points and intervals of uncertainty in the materials recognition is determined by the energy non-homogeneity of the X-ray source. This statement is obvious since in case of single-energy X-ray sources, the identification parameter equals to the ratio between the mass attenuation coefficients for E_H and E_L energies and is not dependent on the mass thickness of the target object.

Therefore, the intentional beam hardening leads to the quality improvement of the materials recognition of objects and their fragments. This conclusion is supported by the preliminary research findings obtained in [1] work, in which physical pre-filtering of high-energy radiation results in beam hardening. In the next section, we shall discuss a number of issues connected with pre-filtering of high-energy radiation in terms of the level line method used for materials recognition.

LEVEL LINE METHOD OF MATERIALS RECOGNITION USING X-RAY RADIATION PREFILTERING

The intentional beam hardening has negative and positive sides. The positive side is the achievement of a principal physical capability of materials recognition within the mass thicknesses range from units to 100 g/cm^2. The negative side of beam hardening is a remarkable reduction in the incident photon flux. This reduction requires to increase the measuring time in view of the original level of measuring error of the recognition parameter.

The above mentioned statements are illustrated by a set of $Q(\rho h)$ dependences with the radiation pre-filtering with lead plates having 5, 10, 15 and 20 mm thickness (Fig. 4).

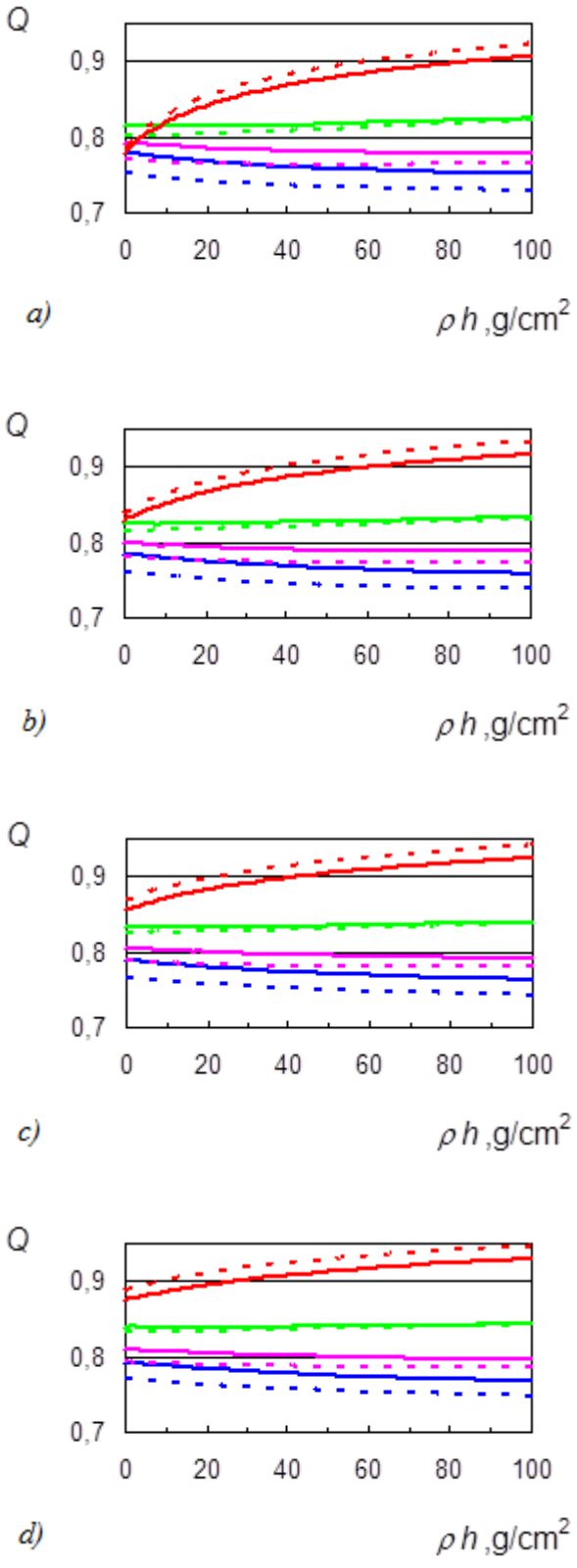

Figure 4: $Q(\rho h)$ dependencies for E_L–E_H energy pairs and Pb filter: a – 5 mm; b – 10 mm; c – 15 mm; d – 20 mm; ——, - - - 4–7.5 and 4.5–9 MeVs, Z=6; ——, - - - 4–7.5 and 4.5–9 MeVs, Z=13; ——, - - - 4–7.5 and 4.5–9 MeVs, Z=26; ——, - - - 4–7.5 and 4.5–9 MeVs, Z=82.

According to Fig. 4, pre-filtering with Pb filter having the thickness more than 15 mm, completely eliminates the intervals of uncertainty. In case of 20 mm thick filter, $Q(\rho h)$ dependencies are almost unaffected by the mass thickness of the object. At the same time, the measuring time should be increased by 2.2 times for 20 mm thick Pb filter. This factor is negative. And no alternative exists for the intentional beam hardening in terms of materials recognition of target objects and their fragments within the whole range of mass thicknesses the consumers are interested in.

In the section below, we shall describe the importance of ADC bit capacity in materials recognition of large-size objects.

BIT CAPACITY SELECTION

Bit capacity selection at the initial range of analog signal

ADC bit capacity is determined by the range of analog signal and the required accuracy of measurements. The cargo inspection systems are initially intended to remotely inspect large-size objects. Presently, the developers face two important and difficult problems concerning the extension of the analog signal range with preservation of the given quality of materials discrimination. In the first problem (9), the extension of the signal range is conditioned by scanning the object with radiant power having nominal and reduced levels. The reduced level of radiant power is used in scanning biological objects. The second problem concerns the increase of mass thickness of target objects and their fragments the materials of which are discriminated correctly up to 200-240 g/cm^2. It is apparent that these problems are equivalent. Thus, the reduction in the radiant power level is proportional to the increase in radiation length of the object.

Let us estimate the impact of ADC bit capacity on the quality of materials recognition. Assume, that the individual scintillator is 6×6 mm^2 in size and 30 mm thick. Radiation pulses of E_L and E_H maximum energies are recorded by 1+1 scheme. Such a scheme provides the maximum efficiency of screening, however, is not optimum for the problem in hand. Similar to the above, these calculations are carried out for the pairs of E_L and E_H maximum energies of 4–7.5 and 4.5-9 MeV, respectively. The coefficient C_Δ is 0,8. The digital signal $C_\Delta(2^k-1)$ corresponds to the maximum level of analog signal. Due to the restrictions described in Section 2, the mass thickness ρh is measured within 20–140 g/cm^2 range.

Figure 5 contains plots of $Q(\rho h)$ dependences obtained for 16-bit ADC. The plot comparison shows that for 4.5-9 MeV E_L-E_H energies, the bit capacity has lower impact on the quality of recognition for objects with thickness not over 100 g/cm^2 than for 4-7.5 MeV E_L-E_H energies. A correct recognition of materials of the four classes in question is impossible for objects with 105 g/cm^2 mass thickness and higher. The natural way out is to employ ADC with a higher bit capacity.

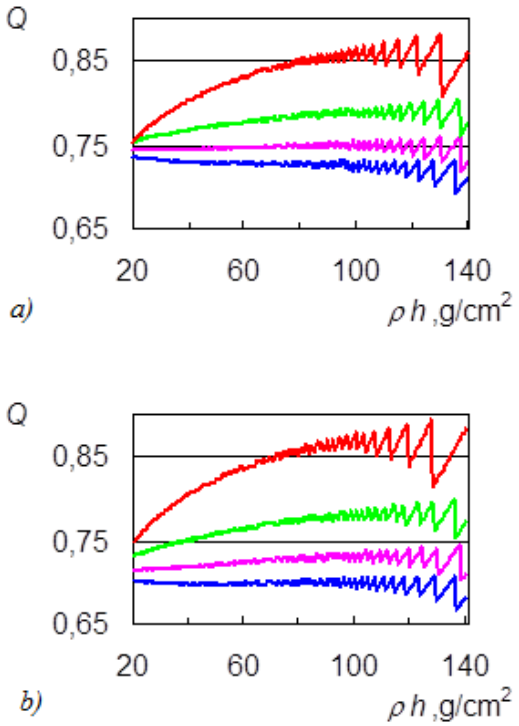

Figure 5: $Q(\rho h)$ dependences for E_L–E_H energy pairs and k=16: a − 4–7.5 MeV; b − 4.5–9 MeV; — Z=6; — Z=13; — Z=26; — Z=82.

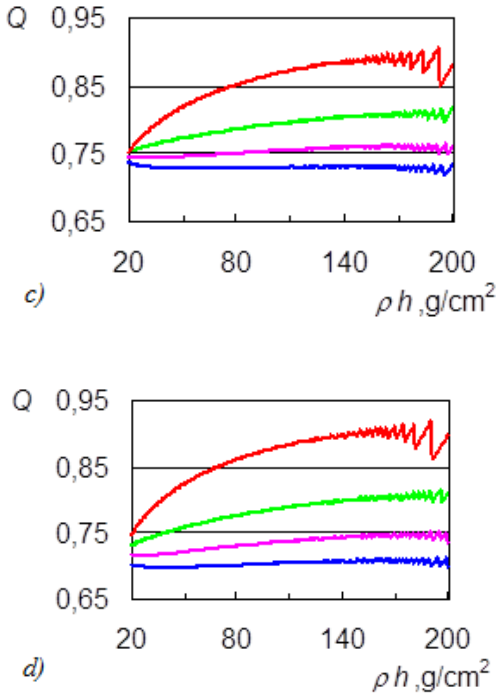

Figure 6: $Q(\rho h)$ dependences for E_L–E_H energy pairs: a − 4–7.5 MeV, k=18; b − 4.5–9 MeV, k=18; c − 4–7.5 MeV, k=20; d − 4.5–9 MeV, k=20; — Z=6; — Z=13; — Z=26; — Z=82.

Figure 6 contains plots of $Q(\rho h)$ dependences obtained for 18- and 20-bit ADCs. The more efficient use of 4.5-9 MeV E_L-E_H energy pair is proved for both of these ADCs. The mass thickness range for objects with the correct materials recognition is extended to 140 g/cm^3 due to the use of 18-bit ADC. For 20-bit ADC, the maximum value of mass thickness achieves 170 g/cm^3 within the thickness range of interest.

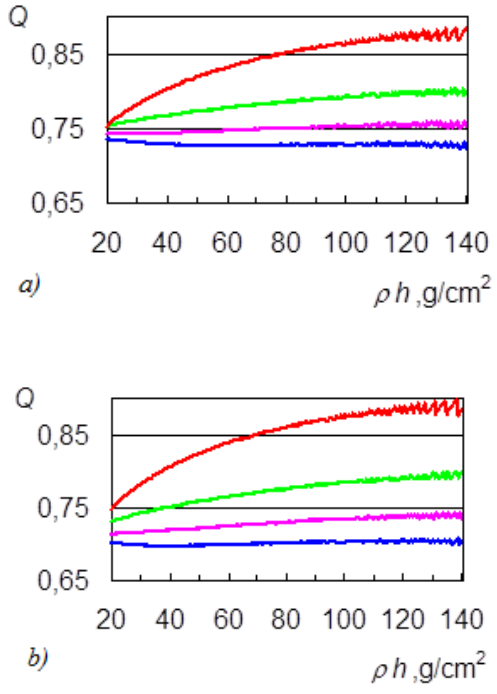

The analog signal range is determined by the ratio between signals travelling through the air and those behind the object with the maximum mass thickness allowing for P_H/P_L ratio and the angular radiation distribution. For E_L-E_H maximum energies of 4.5-9 MeV, the ratio $Y(E_L, \rho h$ = 170 g/cm^2, $Z)/Y(E_L, \rho h$ = 0 g/cm^2, $Z)$ approximates to 3000, while P_H/P_L = 8 in case the ratio between photon flux in the center and in the periphery of the beam is close to 4. At c = 0,8, the maximum value of analog signal exceeds its minimum approx. 120000 times. It should be noted that radiometric non-homogeneity observed in practice, is not taken into account.

Bit capacity selection at narrowed range of analog signal

One of the simplest ways of narrowing the analog signal range is its integration in the maximum X-ray energy E_L [8]. In this case, Y_H and Y_L signals approach to each other. The number of integrating pulses is selected with regard for a possible value excess of the digital signal threshold 2^k–1.

The investigation of the signal range narrowing is accompanied by the construction of $Q(\rho h)$ dependences with recording X-ray pulses with 4-7.5 MeV E_L-E_H energy pair using 1:1 and 3:1 schemes. The latter scheme does not provide a complete pulse matching even for signals travelling through the air. The obtained diagrams are presented in Fig. 7a and 7b.

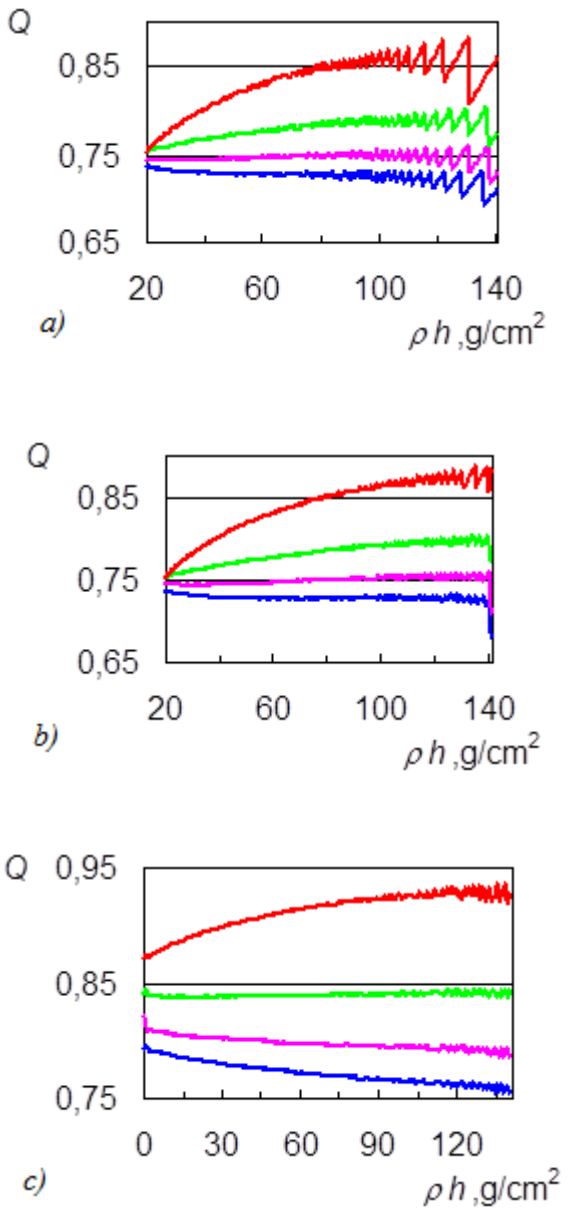

Figure 7: $Q(\rho h)$ dependences, k= 16: a − one pulse at 4 MeV and one pulse at 7.5 MeV; b − three pulses at 4 MeV and one pulse at 7.5 MeV; c − three pulses at 4 MeV and one pulse at 7.5 MeV, 20 mm thick Pb filter: — Z=6; — Z=13; — Z=26; — Z=82.

Figure 7 allows estimating the integration efficiency of analog signal in the lower energy of X-ray radiation. The extension of the thickness range is observed in object fragments the materials of which are effectively discriminated. The additional positive side of this approach is the increased probability of the materials recognition due to the accuracy improvement of Q parameter estimation. The weakest side of this approach is the loss of the inspection efficiency which reduces twice in our case.

The use of X-ray beam hardening filters also reduces the range of analog signal. Figure 7c presents $Q(\rho h)$ dependence for 3:1 scheme of recording X-ray pulses with 4-7.5 MeV E_L-E_H energy pair and 20 mm thick Pb filter. The analog signal integration technique and the use of attenuating filters allow extending the range of mass thickness of object fragments the materials of which are effectively recognized within 0-140 g/cm^2 range.

It is worth noting that $Q(\rho h)$ dependences presented in Fig. 1-7 describe the average functions under research and serve as calibration curves. Another restrictions of materials recognition using the dual energy method refer to scattering of random values $Q(R_L)$ for the material classes in question.

STATISTICAL RESTRICTIONS OF MATERIALS RECOGNITION

The quality of materials recognition using the method of level lines is characterized by the directively given confidence factor γ. This factor is defined by noises in ***Q*** image of the target object. The objects and their fragments should comply with the problem of materials recognition according to their classes and mass thickness range.

The image noises of can be estimated using the approach described in the work [8].

Noise estimation algorithm in Q image

Let us detect the connection between the absolute uncertainty of recognition parameter Q and the main properties of the cargo inspection system.

The mean-square deviation equation for the recognition parameter Q of the target object made of material with Z effective atomic number and ρh mass thickness is written as

$$\sigma Q(R_L(\rho h,Z))=\frac{Q(R_L(\rho h,Z))}{\rho h}\sqrt{\frac{\sigma^2 R_H(\rho h,Z)}{m^2_{\text{int}}(E_H,\rho h,Z)}+\frac{\sigma^2 R_L(\rho h,Z)}{m^2_{\text{int}}(E_L,\rho h,Z)}} \quad (15)$$

Dispersions $\sigma^2 R_L(\rho h, Z)$ and $\sigma^2 R_H(\rho h, Z)$ are found by the incremental decomposition method used for the right-hand sides of (5). It can be assumed that detectors are equivalent; the X-ray source is isotropic; Δ value is small. Hence, dispersions $\sigma^2 R_L(\rho h, Z)$ and $\sigma^2 R_H(\rho h, Z)$ can be expressed as

$$\sigma^2 R_L(\rho h,Z)=\frac{3\sigma^2 Y_L(0,Z)+3\sigma^2 Y_L(\infty,Z)}{(Y_L(0,Z)-Y_L(\infty,Z))^2}+\frac{\sigma^2 Y_L(\rho h,Z)+\sigma^2 Y_L(\infty,Z)}{(Y_L(\rho h,Z)-Y_L(\infty,Z))^2} \quad (16)$$

$$\sigma^2 R_H(\rho h,Z)=\frac{3\sigma^2 Y_H(0,Z)+3\sigma^2 Y_H(\infty,Z)}{(Y_H(0,Z)-Y_H(\infty,Z))^2}+\frac{\sigma^2 Y_H(\rho h,Z)+\sigma^2 Y_H(\infty,Z)}{(Y_H(\rho h,Z)-Y_H(\infty,Z))^2}$$

Measurement times t_L and t_H do not depend on the signal membership in one of the four groups described in Section 2.2.

Equations for dispersions $\sigma^2 Y_L(\rho h,Z)$ and $\sigma^2 Y_H(\rho h,Z)$ are similar to those presented in [8]:

$$\sigma^2 Y_L(\rho h, Z) = ac_L P_L t_L \int_0^{E_L} \overline{E_{ab}^2(E)} f(E, E_L) e^{-m(E,Z)\rho H} \varepsilon(E) dE + \sigma_n^2 t_L \quad (17)$$
$$\sigma^2 Y_H(\rho h, Z) = ac_H P_H t_H \int_0^{E_H} \overline{E_{ab}^2(E)} f(E, E_H) e^{-m(E,Z)\rho H} \varepsilon(E) dE + \sigma_n^2 t_H$$

where $\overline{E_{ab}^2(E)}$ is the average squared energy in the detector remained by the recorded photon with E energy; σ_n^2 is the dispersion of the detector self-noises.

Equations (15)-(17) connect all basic parameters of the cargo inspection system with the mean-square deviation of the recognition parameter Q for each pixel of resulting image.

The analysis of (15)-(17) generates three evident derivations:

$$\begin{aligned} &1.\ \lim_{\rho h \to 0} \sigma Q\big(R_L(\rho h, Z)\big) = \infty; \\ &2.\ \lim_{\rho h \to \infty} \sigma Q\big(R_L(\rho h, Z)\big) = \infty; \\ &3.\ \exists\ \rho h_{\text{opt}},\ \min_{\rho h} \sigma Q\big(R_L(\rho h, Z)\big) = \sigma Q\big(R_L(\rho h_{\text{opt}}, Z)\big) \end{aligned} \quad (18)$$

Calculation example

The behavior of $\sigma Q(\rho h)$ function is studied within its minimum, and a series of calculations was developed for carbon, aluminum, iron, and lead. The analog signals are leveled by the pulse integration using 3:1 scheme (three pulses at 4 MeV and one pulse at 7.5 MeV). For the extension of the recognition range the calculations are provided for 20 mm thick Pb filter. The number of incident quanta is 10^4. Figure 8 presents the obtained $\sigma Q(\rho h)$ dependences.

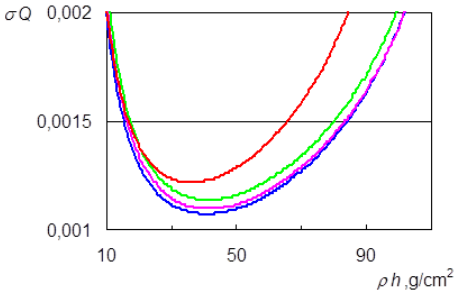

Figure 8: $\sigma Q(\rho h)$ dependences, k=20: three pulses at 4 MeV and one pulse at 7.5 MeV; 20 mm thick Pb filter: — Z=6; — Z=13; — Z=26; — Z=82.

According to Fig. 8, $\sigma Q(\rho h)$ dependences show the explicit minimum and the presence of the mass thickness interval within which the mean-square deviation is not half as much as the minimum. For carbon, aluminum and iron the indicated interval extends from 15 to 80 g/cm^2, while for lead it is 15-65 g/cm^2.

The influence of statistical factor on the quality of the materials recognition is described by $Q(\rho h) \pm 3\sigma Q(\rho h)$ dependences presented in Fig. 9. Dependences $Q(\rho h) - 3\sigma Q(\rho h)$ are illustrated by dash lines, while dependences $Q(\rho h) + 3\sigma Q(\rho h)$ – by solid lines. Calculations are provided for the conditions described in the previous section, with the given number of photons incident on frontal surfaces of detector. In Fig. 9a, the number N_{ph} of incident photons is 10^3, while in Fig. 9b, $N_{ph} = 10^4$.

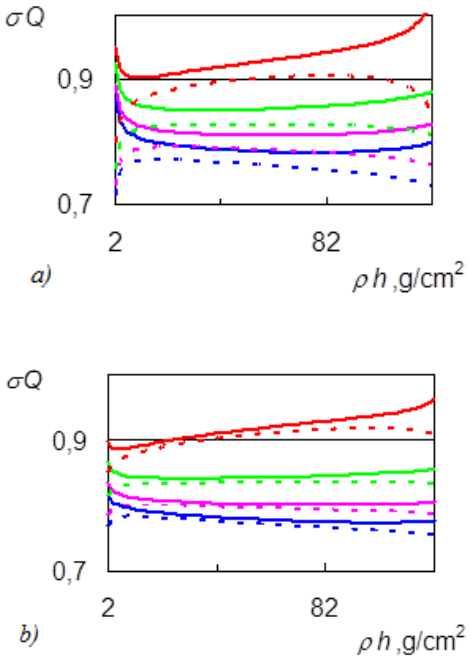

Figure 9: Dependences $Q(\rho h) - 3\sigma Q(\rho h)$ (dash lines) and $Q(\rho h) + 3\sigma Q(\rho h)$ (solid lines), k=20: three pulses at 4 MeV and one pulse at 7.5 MeV; 20 mm thick Pb filter: — Z=6; — Z=13; — Z=26; — Z=82; a – N_{ph}=10^3, b – N_{ph} =10^4.

The fragments having ρh mass thickness and effective atomic numbers of Z_1 and Z_2, $Z_2 > Z_1$, are discriminated with 99.725% probability if the following condition is satisfied:

$$Q(\rho h, Z_1) + 3\sigma Q(\rho h, Z_1) < Q < Q(\rho h, Z_2) - 3\sigma Q(\rho h, Z_2) \quad (19)$$

In Fig. 9a, the intervals at which (19) is not satisfied are very clear. With the increased number of recorded photons, the number of these intervals reduces, and they become narrower. A comparison of the dependences presented in Fig. 9, proves this fact.

It should be noted that besides the increase in the radiant power, the quality of materials recognition can be achieved by the extension of the averaging window when imaging the recognition parameter. This approach is acceptable in case the image of the object fragment contains a significant number of pixels.

CONCLUSIONS

The physical and technical restrictions were investigated in the field of materials recognition of objects and their fragments

using the dual energy method. The thickness range detected for the materials with the different effective atomic numbers possessed the similar recognition parameters. It was shown that the bit capacity of analog-to-digital converters depended on the thickness range of target objects the materials of which were discriminated correctly. Recommendations were given for expanding the application area of the dual-energy method in the materials recognition.

ACKNOWLEDGEMENT

This work was done by contract VIU-66/2016 and with financial support of PowerScan Ltd Company.

REFERENCES

[1] Liu, Y., Sowerby, B.D. and Tickner, J.R., 2008, Comparison of neutron and high-energy X-ray dual-beam radiography for air cargo inspection, Appl. Radiat. Isot., 66: 463-73. https://doi.org/10.1016/j.apradiso.2007.10.005.

[2] Chen, G., Turner, J., Nisius, D., Holt, K. and Brooks, A., 2015, Linatron Mi6, the X-ray source for cargo inspection. Phys. Procedia, 66: 68-74. https://doi.org/10.1016/j.phpro.2015.05.011.

[3] Mandava, A.K. and Regentova, E.E., 2015, Visualization of nuclear and other non-commercial materials using megavoltage X-ray technology, Procedia Comput. Sc., 46: 1268-1273. https://doi.org/10.1016/j.procs.2015.01.048.

[4] Tang, C., 2015, Low energy accelerators for cargo inspection, Reviews of Accelerator Science and Technology, 8: 143-63. http://dx.doi.org/10.1142/S1793626815300008X.

[5] Kolkoori, S., Wrobel, N., Osterloh, K., Redmer, B., Deresch, A. and Ewert, U., 2013, Hoch energie radiografie – erkennung von einzelheiten in großen, komplexen schichttiefen, Mater Test, 55: 683-688. http://dx.doi.org/10.3139/120.110492.

[6] Antolak, A.J., 2015, Overview of accelerator applications for security and defense, Reviews of Accelerator Science and Technology, 8: 27-36. http://dx.doi.org/10.1142/S1793626815300029.

[7] Osipov, S.P., Temnik, A.K. and Chakhlov, S.V., 2014, The effects of physical factors on the quality of the dual high-energy identification of the material of an inspected object, Russ J Nondestruct Test, 50: 491-498. https://doi.org/10.1134/S1061830914080075.

[8] Osipov, S.P., Chakhlov, S.V., Osipov, O.S., Shtein, A.M. and Strugovtsev, D.V., 2015, About accuracy of the discrimination parameter estimation for the dual high-energy method, IOP Conf Ser: Mater Sci Eng, 81: 012082. https://doi.org/10.1088/1757-899X/81/1/012082.

[9] Ogorodnikov, S. and Petrunin, V., 2002, Processing of interlaced images in 4-10 MeV dual energy customs system for material recognition, Phy Rev Accel Beams, 5: 104701. https://doi.org/10.1103/PhysRevSTAB.5.104701.

[10] Gil, Y., Oh, Y., Cho, M. and Namkung, W., 2011, Radiography simulation on single-shot dual-spectrum X-ray for cargo inspection system, Appl. Radiat. Isot., 69: 389-393. https://doi.org/10.1016/j.apradiso.2010.11.011.

[11] Chen, Z.Q., Zhao, T. and Li, L., 2016. A curve-based material recognition method in MeV dual-energy X-ray imaging system. Nucl Sci Tech, 27: 1-8. http://dx.doi.org/10.1007/s41365-016-0019-4.

[12] Rogers, T.W., Jaccard, N. and Griffin, L.D., 2017, A deep learning framework for the automated inspection of complex dual-energy x-ray cargo imagery, Proc. SPIE 10187, Anomaly Detection and Imaging with X-Rays (ADIX) II, 101870L. http://dx.doi.org/10.1117/12.2262662.

[13] Brandis, M., 2013, Development of a gamma-ray detector for z-selective radiographic imaging. PhD abstract thesis. Jerusalem.

[14] Schiff, L.I., 1951, Energy-angle distribution of thin target bremsstrahlung, Phys. Rev., 83: 252-253. https://doi.org/10.1103/PhysRev.83.252.

[15] Ali, E.S.M. and Rogers, D.W.O., 2011, Functional forms for photon spectra of clinical linacs, Phys. Med. Biol., 57: 31-50. https://doi.org/10.1088/0031-9155/57/1/31.

[16] Gamma data for elements. URL: www.ippe.ru/podr/abbn/libr/groupkon.php.

[17] Hubbell, J.H. and Seltzer, S.M., 1995, Tables of x-ray mass attenuation coefficients and mass energy-absorption coefficients 1 keV to 20 MeV for elements Z= 1 to 92 and 48 additional substances of dosimetric interest. NIST Interagency/Internal Report (NISTIR), Gaithersburg, no. PB–95–220539/XAB; NISTIR–5632.

[18] Zav'yalkin, F.M. and Osipov, S.P., 1985, Dependence of the mean value and fluctuations of the absorbed energy on the scintillator dimensions, Sov. Atom. Energy, 59: 281-283. http://doi.org/10.1007/BF01123317.

[19] Li, L., Li, R., Zhang, S., Zhao, T. and Chen, Z., 2016, A dynamic material discrimination algorithm for dual MV energy X-ray digital radiography, Appl. Radiat. Isot., 114: 188-95. https://doi.org/10.1016/j.apradiso.2016.05.018.

[20] Martz, H.E., Glenn, S.M., Smith, J.A., Divin, C.J. and Azevedo, S.G., 2017, Poly-versus mono-energetic dual-spectrum non-intrusive inspection of cargo containers, IEEE Trans. Nucl. Scie., PP: 1-11. http://dx.doi.org/10.1109/TNS.2017.2652455.